RSC Advances

PAPER

View Article Online
View Journal | View Issue

Cite this: *RSC Adv.*, 2020, **10**, 38252

Lanthanide contraction effect and white-emitting luminescence in a series of metal–organic frameworks based on 2,5-pyrazinedicarboxylic acid†

Marina O. Barsukova, *[ab] Sofia V. Cherezova,[ab] Aleksandr A. Sapianik, [ab] Olga V. Lundovskaya,[ab] Denis G. Samsonenko [ab] and Vladimir P. Fedin[ab]

Received 1st September 2020
Accepted 7th October 2020

DOI: 10.1039/d0ra08485a

rsc.li/rsc-advances

A series of lanthanide and yttrium MOFs of two structural types $[M_2(H_2O)_2(nmp)_2(pzc)_3]$ (**1M**) and $[M_2(H_2O)_4(pzc)_3]\cdot NMP\cdot 5H_2O$ (**2M**) (where M – lanthanide or yttrium cation, nmp – *N*-methyl-2-pyrrolidone, pzc^{2-} – 2,5-pyrazinedicarboxylate) was synthesized and characterized by single crystal and powder X-ray diffraction crystallography, TG, elemental analyses and IR-spectroscopy. The effect of lanthanide contraction has led to the fact that lanthanides at the beginning of the series (from lanthanum to gadolinium) have a structure different from the structure of lanthanides at the end of the series and yttrium (from terbium and beyond). According to PXRD patterns of the obtained samples mixed metal materials could be obtained not only as crystalline mixtures of two structure types but also as crystalline products of single structure type. Varying the ratio of lanthanides in the initial reaction mixture allowed us to obtain a wide color range of luminescence, including several near-white-light emitting samples.

Introduction

Materials scientists and chemists showed interest in using lanthanides for obtaining new materials long ago.[1] This was facilitated not only by their unusual luminescent properties as f-elements,[2–4] but also by high coordination numbers, hydrolytic and thermal stability as Lewis acids, and the possibility of being used as catalysts,[5–7] sensors,[8–10] molecular magnets[11,12] and conductive materials.[13] As photoluminescent materials, such compounds have the advantages of high sensitivity of the luminescent response, a wide colour range of emission in the visible region, large values of the Stokes shift, narrow emission bands and high luminescence lifetimes. Among all these applications, the use of mixed metal materials to obtain sources of white-emitting luminescence occupies a special place.[14–16]

MOFs (Metal–Organic Frameworks) are a good platform for producing such materials. MOFs are a "symbiosis" of inorganic nodes with organic linkers forming the "skeleton" of the framework. MOFs have become widely known over the past couple of decades. The interest in their study is primarily due to the wide design possibilities and a large selection of source of organic linkers and metal clusters. There are many possible applications for MOFs in the areas of gas storage and separation,[17–20] heterogeneous catalysis[21,22] and sensing.[23–28] Still one of the most necessary properties for MOFs is high thermal stability and durability over a wide pH range.[29,30]

With the using of rare earth elements into the framework a new subclass was created, named Lanthanide MOFs (LnMOFs) that have demonstrated their uncommon characteristics as catalysts,[31] luminescent sensors,[32–34] white light emitting devices[35,36] as well as their role in biomedical applications.[37] The main source of luminescence properties of LnMOFs called "antenna effect" includes the absorption of light by the organic linkers, followed by an energy transfer to the lanthanide metal ions and subsequent emission by them. Taking this into account the most desirable white light colour could be obtained by the combination of suitable monochromatic emission colours *i.e.* red, green and blue or yellow and blue. There are at least two approaches to obtain white emitting materials using lanthanides: doping of MOFs with lanthanide cations[38] and synthesis of mixed-metal MOFs.[39]

Herein we investigate the lanthanide contraction effect on the formation of series of 3D MOFs of two structural types. We report the solvothermal synthesis of 10 MOFs based on Ln(III), Y(III) and 2,5-pyrazinedicarboxylic acid (H_2pzc) and their mixed metal analogies. Obtained compounds were characterized by single crystal and powder X-ray diffraction, TG and elemental analyses, IR-spectroscopy, ICP-OES (inductively coupled plasma

[a]*Nikolaev Institute of Inorganic Chemistry, Siberian Branch of the Russian Academy of Sciences, 3 Acad. Lavrentiev Ave., 630090, Novosibirsk, Russia. E-mail: barsukova@niic.nsc.ru*

[b]*Novosibirsk State University, 2 Pirogov St., 630090, Novosibirsk, Russia*

† Electronic supplementary information (ESI) available: X-ray crystallography data, IR spectra, PXRD patterns, luminescence spectra and photo of obtained samples. CCDC 2002640 and 2002641. For ESI and crystallographic data in CIF or other electronic format see DOI: 10.1039/d0ra08485a

optical emission spectrometry) and luminescence. It was demonstrated that lanthanide compounds from lanthanum to gadolinium possesses dense 3D structure with no guest molecules while terbium, erbium and yttrium compounds crystallizes into framework with channels filled with guest molecules of NMP and water. The mixed metal materials demonstrate wide colour range of luminescence including near-white-light emitting examples.

Experimental

Materials

All chemicals were of reagent grade (≥95%) and were used as received without further purification. $La(NO_3)_3 \cdot 6H_2O$, $Ce(NO_3)_3 \cdot 6H_2O$, $Pr(NO_3)_3 \cdot 6H_2O$, $Nd(NO_3)_3 \cdot 6H_2O$, $Sm(NO_3)_3 \cdot 6H_2O$, $Eu(NO_3)_3 \cdot 6H_2O$, $Gd(NO_3)_3 \cdot 6H_2O$, $Tb(NO_3)_3 \cdot 6H_2O$, $Er(NO_3)_3 \cdot xH_2O$ was received from STREM Chemicals Inc. (USA), $Y(NO_3)_3 \cdot 6H_2O$ from Dalchem (Russia), 2,5-pyrazinedicarboxylic acid dihydrate from Acros Organics (USA), DMF, *N*-methyl-2-pyrrolidone and concentrated HCl and HNO_3 from Reachem (Russia).

Physical measurements

Powder X-ray diffraction (PXRD) data were collected with Cu-K_α radiation on a powder X-ray diffractometer Shimadzu XRD 7000S. Elemental analyses were performed on the Vario Micro Cube, Elementar. Thermogravimetric analysis (TGA) was performed using TG 209 F1 Iris Thermo Microbalance (NETZSCH) instrument at temperatures between 25 and 600 °C in He atmosphere and a heating rate of 10 °C min^{-1}. FTIR spectra (KBr pellets) were recorded in the range of 4000–400 cm^{-1} on a Scimitar FTS 2000 Fourier-transform infrared spectrometer. The luminescence spectra were recorded on Horiba Jobin Yvon Fluorolog 3 Photoluminescence Spectrometer, equipped with a 450 W xenon lamp, excitation/emission monochromator and FL-1073 PMT detector. Mole fractions of Eu, Tb and Gd in obtained mixed metal samples were determined by ICP-OES (inductively coupled plasma optical emission spectrometry) method using a high-resolution iCAP-6500 (Thermo Scientific, UK) spectrometer with axial view, working in the wavelength range 166–847 nm. The nebulization system consisted of a concentric pneumatic SeaSpray nebulizer and a single-pass cyclonic-type Tracey spray chamber.

Synthetic procedures

Synthesis of compound $[La_2(H_2O)_2(nmp)_2(pzc)_3]$ (1La). A mixture of $La(NO_3)_3 \cdot 6H_2O$ (43.3 mg, 0.1 mmol), $H_2pzc \cdot 2H_2O$ (30.6 mg, 0.15 mmol), NMP (1.5 mL), DMF (0.5 mL) and water (0.5 mL) acidified with concentrated HCl (15 drops) was heated at 100 °C for 1 day in a sealed glass ampule. The obtained colourless crystals were separated by the filtration, washed with DMF (3 × 1 mL) and dried on air. Yield 43 mg (85% based on La). Elemental analysis calculated for $C_{28}H_{28}La_2N_8O_{16}$ (M = 1010.40 g mol^{-1}): C, 33.3; H, 2.8; N, 11.1. Found: C, 33.9; H, 2.7; N, 10.9%. IR (KBr, cm^{-1}): 3170 w, 2971 w, 2931 w, 2882 w, 2363 w, 1633 s, 1610 s, 1509 w, 1477 w, 1424 w, 1394 s, 1376 s, 1315 s, 1252 w, 1206 w, 1175 s, 1113 w, 1040 s, 933 w, 840 m, 825 m, 776 s, 718 m, 670 w, 503 m, 466 m.

Synthesis of compound $[Ce_2(H_2O)_2(nmp)_2(pzc)_3]$ (1Ce). Compound **1Ce** was synthesized according to procedure used for compound **1La**. The obtained yellow crystals were separated by the filtration, washed with DMF (3 × 1 mL) and dried on air. Yield 41 mg (81% based on Ce). Elemental analysis calculated for $C_{28}Ce_2H_{28}N_8O_{16}$ (M = 1012.80 g mol^{-1}): C, 33.2; H, 2.8; N, 11.1. Found: C, 33.1; H, 2.8; N, 11.0%. IR (KBr, cm^{-1}): 3171 w, 2973 w, 2935 w, 2880 w, 2388 w, 1631 s, 1607 s, 1510 w, 1478 w, 1424 w, 1394 s, 1377 s, 1315 s, 1253 w, 1206 w, 1176 s, 1113 w, 1040 s, 934 w, 837 m, 825 m, 776 s, 720 m, 670 w, 531 m, 467 m.

Synthesis of compound $[Pr_2(H_2O)_2(nmp)_2(pzc)_3]$ (1Pr). Compound **1Pr** was synthesized according to procedure used for compound **1La**. The obtained greenish crystals were separated by the filtration, washed with DMF (3 × 1 mL) and dried on air. Yield 42 mg (83% based on Pr). Elemental analysis calculated for $C_{28}H_{28}N_8O_{16}Pr_2$ (M = 1014.80 g mol^{-1}): C, 33.2; H, 2.8; N, 11.0. Found: C, 31.8; H, 3.0; N, 10.7%. IR (KBr, cm^{-1}): 3166 w, 2972 w, 2932 w, 2881 w, 2368 w, 1641 s, 1608 s, 1510 w, 1478 w, 1378 s, 1315 s, 1252 w, 1207 w, 1176 s, 1112 w, 1040 s, 934 w, 838 m, 825 m, 776 s, 722 m, 671 w, 514 m, 468 m.

Synthesis of compound $[Nd_2(H_2O)_2(nmp)_2(pzc)_3]$ (1Nd). Compound **1Nd** was synthesized according to procedure used for compound **1La**. The obtained pale purple crystals were separated by the filtration, washed with DMF (3 × 1 mL) and dried on air. Yield 45 mg (88% based on Nd). Elemental analysis calculated for $C_{28}H_{28}N_8Nd_2O_{16}$ (M = 1021.05 g mol^{-1}): C, 32.9; H, 2.8; N, 11.0. Found: C, 32.6; H, 2.7; N, 10.5%. IR (KBr, cm^{-1}): 3164 w, 2974 w, 2932 w, 2882 w, 2387 w, 1642 s, 1607 s, 1510 w, 1478 w, 1378 s, 1316 s, 1253 w, 1208 w, 1176 s, 1112 w, 1040 s, 934 w, 838 m, 826 m, 776 s, 726 m, 672 w, 515 m, 469 m.

Synthesis of compound $[Sm_2(H_2O)_2(nmp)_2(pzc)_3]$ (1Sm). Compound **1Sm** was synthesized according to procedure used for compound **1La**. The obtained colourless crystals were separated by the filtration, washed with DMF (3 × 1 mL) and dried on air. Yield 45 mg (87% based on Sm). Elemental analysis calculated for $C_{28}H_{28}N_8O_{16}Sm_2$ (M = 1033.30 g mol^{-1}): C, 32.5; H, 2.7; N, 10.8. Found: C, 32.6; H, 2.8; N, 10.4%. IR (KBr, cm^{-1}): 3157 w, 2982 w, 2932 w, 2882 w, 2389 w, 1651 s, 1611 s, 1511 w, 1478 w, 1380 s, 1317 s, 1252 w, 1208 w, 1178 s, 1112 w, 1041 s, 934 w, 841 m, 825 m, 777 s, 729 m, 673 w, 517 m, 472 m.

Synthesis of compound $[Eu_2(H_2O)_2(nmp)_2(pzc)_3]$ (1Eu). Compound **1Eu** was synthesized according to procedure used for compound **1La**. The obtained colourless crystals were separated by the filtration, washed with DMF (3 × 1 mL) and dried on air. Yield 47 mg (91% based on Eu). Elemental analysis calculated for $C_{28}Eu_2H_{28}N_8O_{16}$ (M = 1036.50 g mol^{-1}): C, 32.4; H, 2.7; N, 10.8. Found: C, 31.9; H, 2.8; N, 10.4%. IR (KBr, cm^{-1}): 3154 w, 2975 w, 2933 w, 2882 w, 2379 w, 1653 s, 1614 s, 1510 w, 1477 w, 1380 s, 1318 s, 1253 w, 1209 w, 1178 s, 1114 w, 1041 s, 933 w, 842 m, 825 m, 777 s, 731 m, 670 w, 507 m, 473 m.

Synthesis of compound $[Gd_2(H_2O)_2(nmp)_2(pzc)_3]$ (1Gd). Compound **1Gd** was synthesized according to procedure used for compound **1La**. The obtained colourless crystals were separated by the filtration, washed with DMF (3 × 1 mL) and dried on air. Yield 45 mg (86% based on Gd). Elemental analysis

calculated for $C_{28}Gd_2H_{28}N_8O_{16}$ (M = 1047.07 g mol^{-1}): C, 32.1; H, 2.7; N, 10.7. Found: C, 31.5; H, 2.9; N, 10.1%. IR (KBr, cm^{-1}): 3123 w, 2974 w, 2933 w, 2882 w, 2395 w, 1660 s, 1614 s, 1511 w, 1478 w, 1381 s, 1318 s, 1252 w, 1209 w, 1178 s, 1113 w, 1041 s, 933 w, 842 m, 825 m, 777 s, 734 m, 507 m, 473 m.

Synthesis of compound $[Tb_2(H_2O)_4(pzc)_3]\cdot NMP\cdot 5H_2O$ (2Tb). Compound **2Tb** was synthesized according to procedure used for compound **1La**. The obtained colourless crystals were separated by the filtration, washed with DMF (3 × 1 mL) and dried on air. Yield 49 mg (91% based on Tb). Elemental analysis calculated for $C_{23}H_{33}N_7O_{22}Tb_2$ (M = 1077.40 g mol^{-1}): C, 25.6; H, 3.1; N, 9.1. Found: C, 27.2; H, 3.2; N, 9.6%. IR (KBr, cm^{-1}): 3380 w, 3246 w, 2394 w, 1631 s, 1603 s, 1483 m, 1396 s, 1318 s, 1180 s, 1116 w, 1042 s, 931 w, 843 m, 779 s, 663 w, 518 m, 488 m.

Synthesis of compound $[Er_2(H_2O)_4(pzc)_3]\cdot NMP\cdot 5H_2O$ (2Er). Compound **2Er** was synthesized according to procedure used for compound **1La**. The obtained colourless crystals were separated by the filtration, washed with DMF (3 × 1 mL) and dried on air. Yield 51 mg (93% based on Er). Elemental analysis calculated for $C_{23}Er_2H_{33}N_7O_{22}$ (M = 1094.07 g mol^{-1}): C, 25.2; H, 3.0; N, 9.0. Found: C, 25.5; H, 2.8; N, 9.2%. IR (KBr, cm^{-1}): 3386 w, 3245 w, 2404 w, 1633 s, 1604 s, 1484 m, 1406 s, 1319 s, 1182 m, 1102 w, 1043 s, 931 w, 843 m, 777 s, 780 m, 658 w, 521 m, 492 m.

Synthesis of compound $[Y_2(H_2O)_4(pzc)_3]\cdot NMP\cdot 5H_2O$ (2Y). Compound **2Y** was synthesized according to procedure used for compound **1La**. The obtained colourless crystals were separated by the filtration, washed with DMF (3 × 1 mL) and dried on air. Yield 39 mg (83% based on Y). Elemental analysis calculated for $C_{23}H_{33}N_7O_{22}Y_2$ (M = 1037.38 g mol^{-1}): C, 29.5; H, 3.5; N, 10.5. Found: C, 29.8; H, 3.7; N, 10.4%. IR (KBr, cm^{-1}): 3386 w, 3245 w, 3130 w, 2404 w, 1633 s, 1604 s, 1484 m, 1406 s, 1319 s, 1182 s, 1102 w, 1043 s, 931 w, 843 m, 780 m, 658 w, 521 m, 492 m.

Crystal structure analysis

Diffraction data for the single crystals of compounds **1La** and **2Y** were obtained at 130 K on an automated Agilent Xcalibur diffractometer equipped with a CCD AtlasS2 detector (Mo-K_α, graphite monochromator, ω-scans). Integration, absorption correction, and determination of unit cell parameters were performed using the CrysAlisPro program package.[40] The structures were solved by dual space algorithm (SHELXT)[41] and refined by the full-matrix least squares technique (SHELXL)[42] in the anisotropic approximation (except hydrogen atoms). Positions of hydrogen atoms of organic species were calculated geometrically and refined in the riding model. The crystallographic data and details of the structure refinements are summarized in Table S1.† The selected bond distances and angles for obtained crystal structures are shown in Table S2.† The PLATON/SQUEEZE procedure[43] was employed to calculate the contribution to the diffraction from the solvent region and thereby produced a set of solvent-free diffraction intensities. The formula of **2Y** is derived from SQUEEZE results (87e$^-$ per unit cell), and closely corresponds to the empirical formula of **2Y** obtained from TG and elemental analysis. Crystallographic data for the reported structures have been deposited to the Cambridge Crystallographic Data Centre under the CCDC reference numbers 2002640 and 2002641 for **1La** and **2Y**, respectively. Structure identity of other obtained compounds was proven by PXRD method and by comparison of unit cell parameters (for **1Pr**, **1Eu**, **1Gd**, **2Tb**, see Table S2†).

Preactivation procedure

Samples of as-synthesized compounds **1La** and **2Y** were soaked in acetone for 3 days with changing solvent every day.

Surface area and porous structure

An analysis of the porous structure was performed by a N_2 and CO_2 adsorption technique using Quantochrome's Autosorb iQ at 77 and 195 K, respectively. Initially the compounds were first activated in a dynamic vacuum using standard 'outgas' option of the equipment at 80 °C during 6 hours. Adsorption–desorption isotherms were measured within the range of relative pressures of 10^{-5} to 0.995. The specific surface area was calculated from the data obtained based on the conventional BET model.

Elemental analysis of samples after sorption experiment

Results of elemental analyses for **1La** and **2Y**: calculated for **1La** ($[La_2(H_2O)_2(nmp)_2(pzc)_3]$) $C_{28}H_{28}La_2N_8O_{16}$: C, 33.3; H, 2.8; N, 11.1%; found C, 33.4; H, 2.8; N, 11.1%; calculated for activated **2Y** ($[Y_2(H_2O)_4(pzc)_3]$) $C_{18}H_{14}N_6O_{16}Y_2$: C, 28.9; H, 1.9; N, 11.2%; found C, 29.0; H, 2.1; N, 11.1%.

Synthesis of mixed metal materials

Mixed metal materials from **1** to **22** were synthesized according to procedure used for compound **1La** but using a certain ratio of the starting metal salts, as shown in Table 1. Mole fractions of Eu, Tb and Gd in obtained mixed metal samples were analysed by ICP-OES method. Samples of powder materials (n = 2–3, weight from 2 to 10 mg) were dissolved in concentrated nitric acid and diluted with deionized water. The results of the analysis of the resulting solutions are shown in Table 1.

Results and discussion

Synthesis, structures description and characterization

All compounds were obtained by solvothermal reactions between lanthanide nitrates or yttrium nitrate and 2,5-pyrazinedicarboxylic acid in acidified solvent mixture of NMP, DMF and water.

Compound $[La_2(H_2O)_2(nmp)_2(pzc)_3]$ (**1La**) crystalizes in monoclinic space group $P2_1/c$. An asymmetric unit of **1La** comprises a nine-coordinated La(III) cation, one and a half of pzc^{2-} moiety and coordinated H_2O and NMP molecules (Fig. 1). La(III) cation coordinates four anions, one H_2O and one disordered NMP molecule playing a role of the seven-connecting node. La–O_{COO} bond lengths are 2.456(3), 2.487(3), 2.520(3) and 2.528(3) Å, La–N_{pzc} ones are 2.746(3), 2.783(3) and 2.833(3) Å. La–O_{HOH} bond length is 2.490(3) Å and La–O_{nmp} one is 2.487(3) Å.

Table 1 Composition of pristine and mixed metal samples

	Mole fraction in the reaction mixtures			Mole fraction in the obtained compounds according to ICP-OES		
Sample	Eu	Tb	Gd	Eu	Tb	Gd
1Eu	1	0	0	0.997 ± 0.007	<0.002	<0.002
1Gd	0	0	1	0.0037 ± 0.0003	0.038 ± 0.015	0.95 ± 0.03
2Tb	0	1	0	<0.01	0.988 ± 0.004	0.012 ± 0.004
1	0.9091	0.0909	0	0.84 ± 0.06	0.16 ± 0.01	<0.01
2	0.66(6)	0.33(3)	0	0.72 ± 0.02	0.28 ± 0.02	<0.01
3	0.50	0.50	0	0.537 ± 0.003	0.463 ± 0.003	<0.01
4	0.33(3)	0.66(6)	0	0.37 ± 0.04	63 ± 0.04	<0.01
5	0.0909	0.9091	0	0.150 ± 0.005	0.850 ± 0.005	<0.01
6	0.33(3)	0.33(3)	0.33(3)	0.344 ± 0.004	0.357 ± 0.001	0.299 ± 0.003
7	0.90	0.05	0.05	0.898 ± 0.002	0.056 ± 0.001	0.047 ± 0.001
8	0.50	0.40	0.10	0.49 ± 0.03	0.41 ± 0.05	0.100 ± 0.015
9	0.50	0.10	0.40	0.51 ± 0.02	0.12 ± 0.03	0.36 ± 0.02
10	0.50	0.25	0.25	0.510 ± 0.004	0.26 ± 0.01	0.23 ± 0.02
11	0.40	0.10	0.50	0.38 ± 0.03	0.11 ± 0.01	0.51 ± 0.04
12	0.40	0.50	0.10	0.38 ± 0.03	0.52 ± 0.04	0.100 ± 0.007
13	0.25	0.50	0.25	0.24 ± 0.02	0.51 ± 0.03	0.25 ± 0.02
14	0.25	0.25	0.50	0.25 ± 0.02	0.24 ± 0.02	0.51 ± 0.04
15	0.10	0.50	0.40	0.098 ± 0.009	0.49 ± 0.01	0.41 ± 0.01
16	0.10	0.40	0.50	0.101 ± 0.002	0.388 ± 0.001	0.512 ± 0.002
17	0.05	0.90	0.5	0.042 ± 0.003	0.90 ± 0.06	0.054 ± 0.004
18	0.05	0.05	0.90	0.051 ± 0.006	0.051 ± 0.001	0.898 ± 0.007
19	0.10	0.45	0.45	0.993 ± 0.005	0.43 ± 0.01	0.48 ± 0.01
20	0.10	0.20	0.70	0.097 ± 0.001	0.196 ± 0.002	0.707 ± 0.002
21	0.10	0.30	0.60	0.095 ± 0.001	0.295 ± 0.002	0.609 ± 0.002
22	0.05	0.15	0.80	0.0491 ± 0.001	0.143 ± 0.002	0.807 ± 0.002

Lanthanum cations are connected *via* bridging pzc^{2-} anions to form dense 3D structure. Three of four pzc^{2-} moieties are chelatedly connected. A coordinated water molecule connects free O atoms of ligand carboxylic groups with hydrogen bonds. There are 6-membered rings in structure with La(III) cations as nodes and ligand moieties as edges. Coordinated solvent molecules occupy free volume formed by framework. Guest-accessible volume without coordinated solvent molecules for **1La** was found to be 35% according to PLATON programme package.[43]

Compounds **1Ce–1Gd** are isostructural to **1La** according to PXRD patterns (Fig. 2a) and comparison of unit cell parameters (for **1Pr**, **1Eu** and **1Gd**, see Table S3†). It was shown that unit cell parameters decrease during moving from La to Pr and further to Eu and Gd which is consistent with effect of lanthanide contraction. The structural integrity and phase purity of the crystalline compound was shown by PXRD. Composition of the bulk material was confirmed by IR spectra, elemental and TG analyses (Fig. S1† and 2b). Compounds **1La–1Gd** have similar thermal decomposition behaviour: frameworks are stable up to 300 °C, then removal of coordinated solvent molecules starts. At about 400 °C framework decomposition starts.

Compound $[Y_2(H_2O)_4(pzc)_3]\cdot NMP\cdot 5H_2O$ (**2Y**) crystalizes in triclinic space group $P\bar{1}$. An asymmetric unit of **2Y** comprises a nine-coordinated Y(III) cation, one and a half of pzc^{2-} moiety and coordinated H_2O molecules. Y(III) cation coordinates four pzc^{2-} anions and two H_2O molecules (Fig. 3). Y–O_{COO} bond lengths are 2.294(2), 2.310(2), 2.3602(19) and 2.377(2) Å, Y–N_{pzc} are 2.604(2), 2.638(2) and 2.740(2) Å. Y–O_{HOH} bond lengths are 2.360(2) and 2.371(2) Å. All bond distances for compound **2Y** are about 0.1 Å shorter then corresponding bonds in compound

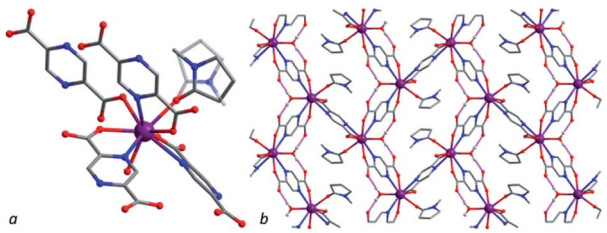

Fig. 1 (a) The coordination environment of La(III) cations in **1La**. H atoms are omitted. (b) Structure view along *a*. H atoms of organic linker and coordinated NMP molecule are omitted. La atoms are shown purple; C, grey; N, blue, O, red. H atoms of water molecule are shown in light grey. Hydrogen bonds are shown in magenta.

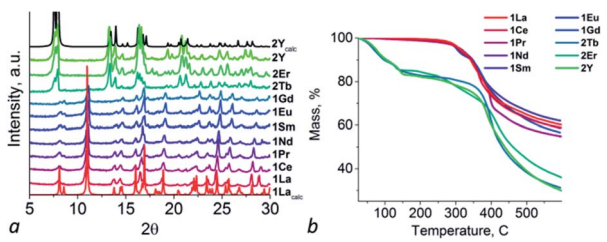

Fig. 2 (a) PXRD patterns for obtained compounds **1La–2Y**. (b) TG curves for **1La–2Y**.

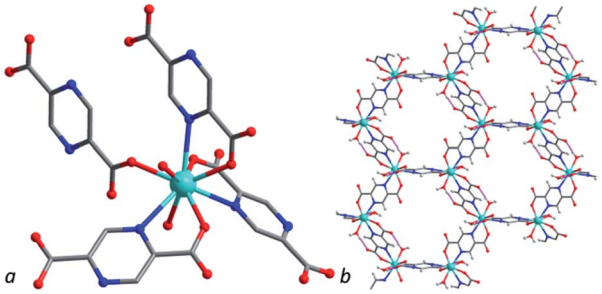

Fig. 3 (a) The coordination environment of Y(III) cations in **2Y**. H atoms are omitted. (b) Structure view along *a*. Hydrogen bonds are shown in magenta. Y atoms are shown cyan; C, grey; N, blue, O, red, H, light grey.

1La that in a good agreement with difference in cationic radii. Bridging pyrazinedicarboxylates form a 3D structure with hexagonal channels along *a* axis. Guest-accessible volume for **2Y** was found to be 35% according to PLATON programme package.[43] Guest composition was determined and confirmed by combination of single crystal X-ray diffraction data, IR spectroscopy, elemental and TG analyses (Fig. 2 and S1†). Framework with the structure similar to **2Y** was obtained using Tm(III) as metal source.[44]

According to TG the first step (under about 150 °C) involves the removal of guest solvent molecules of NMP and water (calculated for one NMP and five H_2O 20%, found 18%). After about 350 °C decomposition of the framework starts.

Compounds **2Er** and **2Tb** are isostructural to **2Y** according to PXRD patterns and unit cell parameters measurements (Fig. 2a and Table S3†). According to elemental and TG analyses compound **2Tb** has formula $[Tb_2(H_2O)_4(pzc)_3]\cdot NMP\cdot 5H_2O$ and compound **2Er** has formula $[Er_2(H_2O)_4(pzc)_3]\cdot NMP\cdot 5H_2O$. Both compounds have TG curves similar to **2Y** one. On the first step upon heating both compounds lose guest solvent molecules (calculated for **2Tb** 17%, found 17%, calculated for **2Er** 17%, found 15%).

IR spectra are very similar for all 10 compounds (Fig. S1†). Broad bands for free O–H and C–H stretching vibrations are present in a range between 2800 and 3500 cm^{-1}. Strong vibration bands of double C=O bonds are observed from 1633 to 1660 (asymmetric stretch) and from 1610 to 1614 cm^{-1} (symmetric stretch) from La to Gd. Moreover the position of the bands is shifted by increasing the atomic number of the element in the periodic table. For compounds **2Tb**, **2Er** and **2Y** vibration bands of double C=O bonds are observed on 1631–1633 and 1603–1604 cm^{-1}. Vibrations of C–N bond of ligand and NMP cation are visible at about 1175–1180 cm^{-1} for all compounds.

BET surface characterization of selected compounds was carried out. Samples of **1La** and **2Y** were preactivated by exchanging of as-synthesized guest molecules with acetone and then degassed under dynamic vacuum with heating at 80 °C during 6 hours. Obtained isotherms of N_2 at 77 K and CO_2 at 195 K are shown in Fig. S2.† Analysis of obtained isotherms demonstrates that both compound adsorbs small amounts of gases and appear to be unporous. Calculated BET surface areas reach 7 $m^2\ g^{-1}$ (CO_2) and 6 $m^2\ g^{-1}$ (N_2) for **1La** and 11 $m^2\ g^{-1}$ (CO_2) and 8 $m^2\ g^{-1}$ (N_2) for **2Y**. According PXRD patterns (Fig. S3†) and elemental analyses of samples after sorption both compounds save their crystal structures but still contain coordinated solvent molecules of NMP and water while **2Y** loses its guest molecules. Although both compounds save their structure after activation they cannot be used as sorbents due to inaccessibility of inner surface because of irremovable coordinated solvent molecules (**1La** and **2Y**) and too small pore entrance (**2Y**). Activation under more stringent conditions leads to degradation of the framework.

Mixed metal materials (**1–22**) were synthesized using certain molar ratio of two lanthanide salts of Eu and Tb and three lanthanide salts of Eu, Gd and Tb in starting reaction mixture. In the first case Eu and Tb were chosen to complete RGB colour model to reach white-emitting material where Eu gives red colour luminescence, Tb – green and ligand has own intraligand luminescence of blue colour. Mole fractions of Eu and Tb in obtained materials were obtained using ICP-OES method and appear to be the same with mole fractions in reaction mixture (Table 1).

It was shown that PXRD patterns of bimetallic mixed metal materials save crystal structure of Eu compound (**1Eu**) for molar ratios of Eu to Tb from 10 : 1 to 1 : 1 (from sample **1** to sample **3**) and structure of Tb compound (**2Tb**) in case of greater influence of Tb for molar ratio 1 : 10 (for sample **5**). Only in case of molar ratio of Eu to Tb 1 : 2 (sample **4**) PXRD pattern of resulting material contains peaks corresponding to both crystal structure (Fig. 4). It could be concluded that europium has a more intensive effect on the resulting structure of mixed metal framework in case of bimetallic mixed metal materials.

In the case of three-metallic materials PXRD patterns of mixed metal materials changes steadily from dense structure (for higher sum of molar ratio of Eu and Gd) to porous framework (for samples with higher Tb molar ratio) (Fig. S4†). Samples **7**, **8**, **9**, **10** and **11** with the highest mole fraction of Eu from 0.9 to 0.4 and low mole fraction of Tb up to 0.4 expectedly have structure of compound **1Eu**. The corresponding samples with "mirror" mole fraction of Gd (see Table S4†) have structure of **1Gd** only in case of sample **14**, structure of **2Tb** in case of sample **16** and mix of both structure types in case of sample **18**. Thus it could be concluded that despite of the fact that Eu- and Gd-containing compounds crystallizes in one structure type their influence in three-metal system is significantly differs.

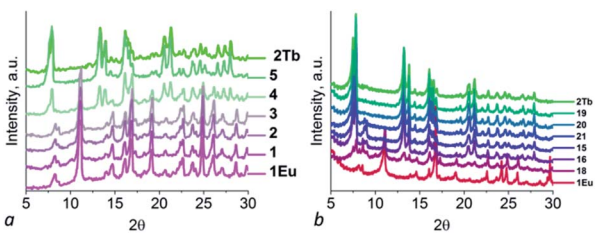

Fig. 4 PXRD patterns for samples **1–5** (a) and **15**, **16**, **18**, **19**, **20**, **21** (b) in comparison with **1Eu** and **2Tb**.

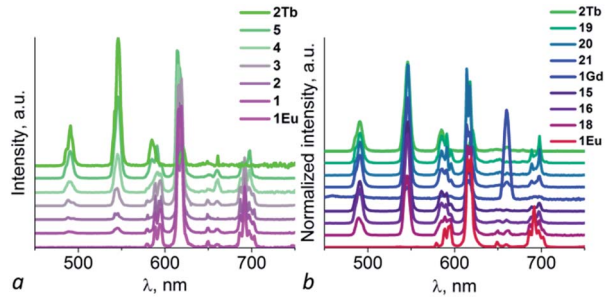

Fig. 5 Luminescence spectra for mixed metal samples in comparison with **1Eu**, **1Gd** and **2Tb** ones. (a) Emission spectra for Eu/Tb mixed metal series, $\lambda_{ex} = 330$ nm. (b) Emission spectra for Eu/Tb/Gd mixed metal series, $\lambda_{ex} = 330$ nm.

Only three mixed metal samples **17**, **19** and **20** have structure of **2Tb**. There is a mix of two structure types in all other cases.

Photoluminescence properties

The solid-state luminescent properties of obtained samples were explored at room temperature, and the emission spectra were given in Fig. 5 and S5.† Compound **1Eu** and **2Tb** display bright red and green luminescence under UV irradiation, respectively. Compound **1Gd** presents a weak blue luminescence. The solid-state luminescent spectra of **1Eu**, excited at 330 nm, shows the narrow emission peaks at about 579, 594, 619, 649 and 692 nm, originating from $^5D_0 \rightarrow {}^7F_0$, $^5D_0 \rightarrow {}^7F_1$, $^5D_0 \rightarrow {}^7F_2$, $^5D_0 \rightarrow {}^7F_3$ and $^5D_0 \rightarrow {}^7F_4$ f–f transitions of Eu^{3+} ions, respectively, in which the electric dipole transition $^5D_0 \rightarrow {}^7F_2$ dominates the red colour emission. Compound **1Gd** reveals narrow peaks at 545, 589, 616, 660 and 694 nm ($\lambda_{ex} = 330$ nm), corresponding to the characteristic transitions of $^5D_0 \rightarrow {}^7F_0$, $^5D_0 \rightarrow {}^7F_1$, $^5D_0 \rightarrow {}^7F_2$, $^5D_0 \rightarrow {}^7F_3$ and $^5D_0 \rightarrow {}^7F_4$ of Gd^{3+} ions, respectively. Compound **2Tb** reveals narrow peaks at 491, 546, 585, 621 and 661 nm ($\lambda_{ex} = 330$ nm), corresponding to the characteristic transitions of $^5D_4 \rightarrow {}^7F_6$, $^5D_4 \rightarrow {}^7F_5$, $^5D_4 \rightarrow {}^7F_4$, $^5D_4 \rightarrow {}^7F_3$ and $^5D_4 \rightarrow {}^7F_2$ of Tb^{3+} ions, respectively. The strongest peak at 546 nm produces the green colour emission for **2Tb**. The ligand-centred emission is completely absent in the emission bands of **1Eu–2Tb**, implying efficient energy transfer from H_2pzc to lanthanide ions *via* "antenna effect".

Mixed metal materials of different Eu and Tb molar ratios demonstrate colour range from green to red while Eu/Tb/Gd samples have wide colour range under irradiation with $\lambda_{ex} =$ 365 nm including not only green and red, but also near-white-light emitting samples (Fig. 6 and S6†). Dominant influence of Eu(III) cations is appeared to have key role not only in formation of crystal structure of the first type (**1Eu**) but also in emission spectra of ternary mixed metal materials **6–14** (Eu mole fraction from 0.90 to 0.25) which have emission spectra in the region of red colour. For selected samples with near-white-light luminescence QY were measured (Table 2). The highest QY among mixed metal materials were obtained for samples **15** (21.1%), **16** (23.7%), **20** (24.3%) and **21** (26.8%). Samples **15**, **16**, **17**, **18**, **19**, **20**, **21** and **22** have the closest to white-light point

Table 2 Quantum yield for selected obtained samples

Sample	Quantum yield, %
1Eu	16.90 ± 0.01
2Tb	26.40 ± 0.01
1	15.15 ± 0.01
2	9.61 ± 0.02
3	14.02 ± 0.01
4	12.08 ± 0.02
5	14.77 ± 0.01
15	21.09 ± 0.02
16	23.73 ± 0.02
17	15.34 ± 0.01
18	17.10 ± 0.01
19	16.26 ± 0.02
20	24.34 ± 0.02
21	26.81 ± 0.02
22	17.28 ± 0.02

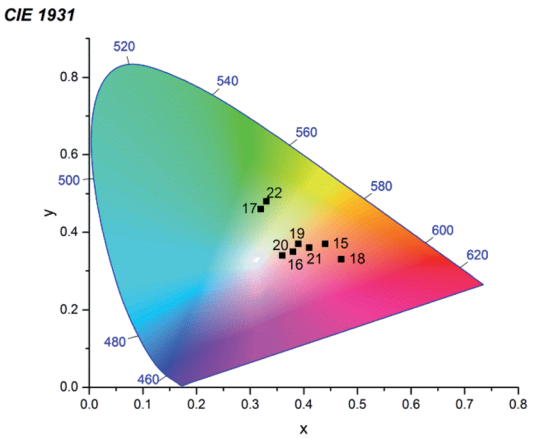

Fig. 7 CIE 1931 plot of samples **15–22**, $\lambda_{ex} = 365$ nm.

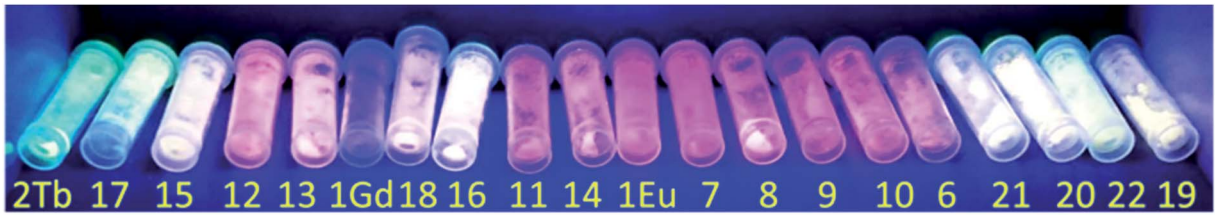

Fig. 6 Photo of samples Eu/Tb/Gd mixed metal series under UV light, $\lambda_{ex} = 365$ nm.

(0.33, 0.33) CIE coordinates among all obtained samples (Fig. 7). Taking into account that only samples **19** and **20** could be obtained as pure crystalline phase of the second structure type (according to PXRD pattern) these material could be considered the most promising for creating of luminophores for WLED from UV-LEDs.

Conclusions

In summary we synthesized a series of new coordination polymers based on Ln(III) and 2,5-pyrazinedicarboxylic acid and demonstrated the influence of lanthanide contraction effect on the their structure. It was demonstrated that compounds with lanthanides from lanthanum to gadolinium possesses dense 3D structure with no guest molecules while terbium, erbium and yttrium compounds crystallizes into framework with channels filled with guest molecules of NMP and water. The mixed metal materials demonstrate wide colour range of luminescence including near-white-light emitting examples.

Conflicts of interest

There are no conflicts to declare.

Acknowledgements

The reported study was funded by The Russian Science Foundation according to the research project no. 19-73-00169.

References

1 S. A. Cotton and P. R. Raithby, *Coord. Chem. Rev.*, 2017, **340**, 220.
2 A. M. Nonat and L. Charbonnière, *Coord. Chem. Rev.*, 2020, **409**, 213192.
3 X. Chen, T. Sun and F. Wang, *Chem.–Asian J.*, 2020, **15**, 21.
4 J.-C. G. Bünzli, *Coord. Chem. Rev.*, 2015, **293–294**, 19.
5 A. R. Richard and M. Fan, *J. Rare Earths*, 2018, **36**, 1127.
6 A. D. G. Firmino, F. Figueira, J. P. C. Tomé, F. A. Almeida Paz and J. Rocha, *Coord. Chem. Rev.*, 2018, **355**, 133.
7 H. Pellissier, *Coord. Chem. Rev.*, 2017, **336**, 96.
8 M. L. Aulsebrook, B. Graham, M. R. Grace and K. L. Tuck, *Coord. Chem. Rev.*, 2018, **375**, 191.
9 Y. Hasegawa and Y. Kitagawa, *J. Mater. Chem. C*, 2019, **7**, 7494.
10 K. Staszak, K. Wieszczycka, V. Martur and B. Tylkowski, *Coord. Chem. Rev.*, 2019, **397**, 76.
11 J.-H. Jia, Q.-W. Li, Y.-C. Chen, J.-L. Liu and M.-L. Tong, *Coord. Chem. Rev.*, 2019, **378**, 365.
12 Z. Zhu, M. Guo, X.-L. Lia and J. Tang, *Coord. Chem. Rev.*, 2019, **378**, 350.
13 L. S. Xie and M. Dincă, *Isr. J. Chem.*, 2018, **58**, 1119.
14 Z.-Y. Zhou, Y.-H. Han, X.-S. Xing and S.-W. Du, *ChemPlusChem*, 2016, **81**, 798.
15 A. Tiwari and S. J. Dhoble, *Luminescence*, 2020, **35**, 4.
16 Z. Zhang, Y. Chen, H. Chang, Y. Wang, X. Li and X. Zhu, *J. Mater. Chem. C*, 2020, **8**, 2205.
17 S. Qiu, M. Xue and G. Zhu, *Chem. Soc. Rev.*, 2014, **43**, 6116.
18 K. Adil, Y. Belmabkhout, R. S. Pillai, A. Cadiau, P. M. Bhatt, A. H. Assen, G. Maurin and M. Eddaoudi, *Chem. Soc. Rev.*, 2017, **46**, 3402.
19 D. Alezi, Y. Belmabkhout, M. Suyetin, P. M. Bhatt, Ł. J. Weseliński, V. Solovyeva, K. Adil, I. Spanopoulos, P. N. Trikalitis, A.-H. Emwas and M. Eddaoudi, *J. Am. Chem. Soc.*, 2015, **137**, 13308.
20 I. A. Ibarra, J. W. Yoon, J. Chang, S. K. Lee, V. M. Lynch and S. M. Humphrey, *Inorg. Chem.*, 2012, **51**, 12242.
21 L. Zhu, X.-Q. Liu, H.-L. Jiang and L.-B. Sun, *Chem. Rev.*, 2017, **117**, 8129.
22 Y.-B. Huang, J. Liang, X.-S. Wang and R. Cao, *Chem. Soc. Rev.*, 2017, **46**, 126.
23 T. N. Nguyen, F. M. Ebrahim and K. C. Stylianou, *Coord. Chem. Rev.*, 2018, **377**, 259.
24 Z. Hu, B. J. Deibert and J. Li, *Chem. Soc. Rev.*, 2014, **43**, 5815.
25 A. Douvali, A. C. Tsipis, S. V. Eliseeva, S. Petoud, G. S. Papaefstathiou, C. D. Malliakas, I. Papadas, G. S. Armatas, I. Margiolaki, M. G. Kanatzidis, T. Lazarides and M. J. Manos, *Angew. Chem., Int. Ed.*, 2015, **54**, 1651.
26 B. Gole, A. K. Bar and P. S. Mukherjee, *Chem.–Eur. J.*, 2014, **20**, 2276.
27 S. G. Dunning, A. J. Nunez, M. D. Moore, A. Steiner, V. M. Lynch, J. L. Sessler, B. J. Holliday and S. M. Humphrey, *Chem*, 2017, **2**, 579.
28 I. A. Ibarra, T. W. Hesterberg, J. Chang, J. W. Yoon, B. J. Holliday and S. M. Humphrey, *Chem. Commun.*, 2013, **49**, 7156.
29 B. Liu, K. Vikrant, K.-H. Kim, V. Kumar and S. K. Kailasa, *Environ. Sci.: Nano*, 2020, **7**, 1319.
30 S. Yuan, L. Feng, K. Wang, J. Pang, M. Bosch, C. Lollar, Y. Sun, J. Qin, X. Yang, P. Zhang, Q. Wang, L. Zou, Y. Zhang, L. Zhang, Y. Fang, J. Li and H.-C. Zhou, *Adv. Mater.*, 2018, **30**, 1704303.
31 C. Pagis, M. Ferbinteanu, G. Rothenberg and S. Tanase, *ACS Catal.*, 2016, **6**, 6063.
32 X. H. Huang, L. Shi, S. M. Ying, G. Y. Yan, L. H. Liu, Y. Q. Sun and Y. P. Chen, *CrystEngComm*, 2018, **20**, 189.
33 J. Wang, Q.-S. Zhang, W. Dou, A. M. Kirillov, W.-S. Liu, C. Xu, C.-L. Xu, R. Fang and L.-Z. Yang, *Dalton Trans.*, 2018, **47**, 465.
34 Z. Hu, G. Huang, W. P. Lustig, F. Wang, H. Wang, S. J. Teat, D. Banerjee, D. Zhang and J. Li, *Chem. Commun.*, 2015, **51**, 3045.
35 Y. Gai, Q. Guo, K. Xiong, F. Jiang, C. Li, X. Li, Y. Chen, C. Zhu, Q. Huang, R. Yao and M. Hong, *Cryst. Growth Des.*, 2017, **17**, 940.
36 J.-J. Yu, W.-J. Liang, Q. Zhang, M.-M. Li and D.-H. Qu, *Chem.–Asian J.*, 2019, **14**, 3141.
37 T.-T. Zheng, J. Zhao, Z.-W. Fang, M.-T. Li, C.-Y. Sun, X. Li, X.-L. Wang and Z.-M. Su, *Dalton Trans.*, 2017, **46**, 2456.
38 Y. Li, T. Jing, G. Xu, J. Tian, M. Dong, Q. Shao, B. Wang, Z. Wang, Y. Zheng, C. Yang and Z. Guo, *Polymer*, 2018, **149**, 13.
39 S. Abednatanzi, P. G. Derakhshandeh, H. Depauw, F.-X. Coudert, H. Vrielinck, P. Van Der Voort and K. Leus, *Chem. Soc. Rev.*, 2019, **48**, 2535.

40 *CrysAlisPro 1.171.40.74a*, Rigaku Oxford Diffraction, The Woodlands, TX, 2019.
41 G. M. Sheldrick, *Acta Crystallogr., Sect. A: Found. Adv.*, 2015, **71**, 3.
42 G. M. Sheldrick, *Acta Crystallogr., Sect. C: Cryst. Struct. Commun.*, 2015, **71**, 3.
43 A. L. Spek, *Acta Crystallogr., Sect. C: Cryst. Struct. Commun.*, 2015, **71**, 9.
44 Y. Pan, D. Ma, H. Liu, H. Wu, D. Hec and Y. Li, *J. Mater. Chem.*, 2012, **22**, 10834.